Zoom-in simulations of galaxies: connecting metallicities and star formation histories

Autor: Andrés Vicente Arévalo
Supervisor: Arianna Di Cintio
Co-Supervisor: Chris Brook

Universidad de La Laguna
Máster de Astrofísica
2019-2020

Index

Resumen

Este Trabajo Fin de Máster está basado en el análisis e implementación de simulaciones de galaxias a alta resolución. Empezaremos haciendo un repaso a las técnicas y a la base teórica usada para realizar las simulaciones: concepto de simulación de N cuerpos y tipos de partículas utilizadas 1.1, algoritmos para la aceleración del cálculo de las interacciones gravitatorias 1.2, introducción de las ecuaciones hidrodinámicas en simulaciones de N cuerpos (formalismo de *smooth particle hydrodinamics*) 1.3, mecanismos de formación estelar 1.4 y retroalimentación 1.5 en simulaciones y una pequeña exposición del código con el que realizaremos dichas simulaciones 1.6. A su vez, haremos una breve descripción de varias simulaciones realizadas previamente con las mismas técnicas (sección 1.7). Estas simulaciones las usaremos posteriormente para analizar la evolución química de las galaxias y su relación con la historia de formación estelar de dichas galaxias.

Para la implementación de las simulaciones se ha hecho uso de un código de simulaciones de N cuerpos e hidrodinámicas preexistente (ChaNGa, Thomas Quinn 2013 [18]), optimizado para simulaciones cosmológicas y con implementación de retroalimentación de agujeros negros (Harshitha Menon et. al. 2018 [19]). Por rapidez y sencillez, se han escogido condiciones iniciales de una galaxia enana de `NIHAO` (proyecto donde se simularon 100 galaxias a alta resolución con masas de 10^9 a $10^{12} M_\odot$. Liang Wang et. al. 2016 [14]) para realizar el proceso de depuración del código y corregir algunas de las incompatibilidades que han surgido durante el proceso de instalación. Los parámetros cosmológicos utilizados son los obtenidos por Plank collaboration et. al. 2019 [1], explicados más en detalle en la sección 3.3. Próximamente se pasará a ejecutar simulaciones análogas pero con las condiciones iniciales del grupo local (CLUES: Constrained Local UniversE Simulations, G. Yepes et. al. 2009 [31]) que nos permitan estudiar el origen y las interacciones de los diferentes componentes del mismo.

Todo esto se ha realizado en el superordenador de La Palma con ayuda del soporte técnico y de los desarrolladores del código como se explica en la sección 3.2. Una vez ha sido instalado todo el software necesario, se ha procedido a correr diferentes simulaciones con distintos parámetros y a comparar preliminarmente los resultados para cerciorarnos del correcto funcionamiento del código. Las primeras simulaciones han sido ejecutadas (hasta $z \sim 3$) y muestran un comportamiento satisfactorio en cuanto al hecho de mostrar consistencia entre distintas ejecuciones con diferentes resoluciones temporales, así como a la hora de mostrar el comportamiento esperado en la jerarquía de formación de estructuras para la cosmología utilizada del paradigma ΛCDM.

Por otra parte, se han analizado simulaciones previas en busca de relaciones entre la metalicidad estelar y la historia de formación estelar de la galaxia a la que pertenecen. Esto se ha hecho cogiendo una muestra de galaxias de distintas masas de los proyectos `NIHAO` (Liang Wang et.al. 2016 [14]) y `MAGICC` (G. S. Stinson et. al. [28]) representativa en base a los diferentes espectros de masa (Galaxias tipo Vía Láctea $M \sim 10^{11-12} M_\odot$,

galaxias pequeñas $M \sim 10^{9-10} M_{\odot}$ y galaxias enanas $M \sim 10^{8-9} M_{\odot}$) y representativa también dentro de las diferentes historias de acreción. Esto se ha llevado a cabo infiriendo la historia de acreción en base a los gráficos de evolución química y de eficiencia de formación estelar (figuras 6, 5 y 8), donde se pueden observar los diferentes eventos de acreción (si los hay) que ha sufrido cada galaxia.

Sobre esta muestra se han desarrollado distintas rutinas de python donde, a partir de las diferentes instantáneas de las simulaciones, se han calculado parámetros como: la historia de formación estelar, la eficiencia de dicha formación estelar y la variación de la composición química con diferentes trazadores (Hidrógeno, Oxigeno, Hierro y sus cantidades relativas). Los diferentes elementos químicos presentes dan indicaciones de las diferentes tendencias de la formación estelar al estar relacionados con distintos eventos como supernovas tipo Ia o tipo II (secciones 4.3 y 4.4). Con estos datos extraídos de las simulaciones se ha representado la evolución quimica de las galaxias en los diferentes trazadores ($[O/Fe]$: figura 6, $[Fe/H]$: figura 5), así como la evolución de la formación estelar (figura 8). A su vez, estos cálculos han servido para construir un espacio de parámetros ($[O/Fe]$ - $[Fe/H]$: figura 7) donde se ve reflejada de forma implícita la historia de formación y evolución de las galaxias. El análisis descrito ha permitido identificar diferentes tendencias en las simulaciones que indican que la historia de formación estelar , la masa de la galaxia y la historia de acreción de la misma son los principales condicionantes a la hora de determinar el contenido químico de la galaxia resultante. A su vez, la historia de formación estelar esta condicionada por la masa de la galaxia y la historia de acreción, como se explica en la sección 4.4.

Todo esto puede ser especialmente relevante a la hora de inferir historias de formación estelar o historias de acreción de galaxias observadas. Si tenemos en cuenta que los modelos utilizados para el análisis reproducen las propiedades de galaxias reales (como muestran los trabajos de Tobias Buck et. al. 2020 [25] y Chris B. Brook et.al. 2020 [26]), podemos acotar los posibles procesos de acreción y la posible historia de formación que han sufrido las galaxias observadas basándonos en las correlaciones mostradas en este trabajo.

Por último, se da una breve explicación del trabajo que está actualmente en desarrollo en ambos frentes, tanto en las ejecuciones de nuevas simulaciones como en el análisis de las mismas. En el ámbito de ejecución de nuevas simulaciones se están ultimando los detalles para ejecutar simulaciones de todo un grupo local con la infraestructura de *software* desarrollada en este trabajo una vez se hayan solventado algunas dificultades técnicas actuales. En el aspecto del análisis de las simulaciones previas, se está trabajando para ver más en detalle cómo se han enriquecido en metales las partículas de gas que han dado lugar a las estrellas observadas en la simulación con el fin de comprender mejor el ciclo bariónico y como la recirculación del gas y la acreción de nuevo material afecta a la formación de galaxias.

1 Introduction

In this section we will present the theoretical background and techniques used to make the simulations. We will describe the main idea of the N-Body simulations (1.1) as well as some complementary techniques that allow us to simulate with high fidelity the evolution of a galaxy. These techniques are Smooth Particle Hydrodynamics (SPH 1.3) and the formation and evolution of the stars within the simulations and how this affects the chemical abundances (1.4, 1.5). Also a brief description to the code we are going to use (1.6) and a overview of the previous simulations (1.7).

1.1 N-Body simulations

N-Body simulations consist in evolving a system with N particles solving a set of equations that describe their interactions. This type of simulations are widely used in Astrophysics since the problem of integrating a set of non-linear second order ordinary differential equations relating the acceleration $\partial\vec{r_i}/\partial t^2 = \vec{F_i}/m_i$ can only be solved numerically for a $N > 2$.

In our case, we are going to solve the gravitational interaction mainly, to see how, from some initial conditions given by cosmological constrains we are able to form and evolve halos of dark matter (DM) with a baryon component (galaxies) in its center. For that purpose, we are going to use the current ΛCDM paradigm (with the parameters of Plank collaboration et. al. 2019 [1]), which give us the most accurate description of which properties our particles must have and the interactions that we need to solve between them in order to achieve a simulation that better resembles the observed Universe. The equations to be solved in this case (eq. 1) are the Newtonian's equations of motion with a few modifications to ensure both the efficiency and accuracy of the solution.

$$\vec{F_i} = -\sum_{j\neq i} \frac{G m_i m_j (\vec{r_i} - \vec{r_j})}{(|\vec{r_i} - \vec{r_j}|^2 + \epsilon^2)^{3/2}} \tag{1}$$

Where G is the gravitational constant, $m_i, \vec{r_i}$ are the mass and position of the i particle and ϵ is a positive constant called the smoothing length. The smoothing or softening length sets the scale below which the gravitational interaction is suppressed in order to avoid the singularity of the Newton's equations in close encounters between particles and the artificial formation of binary systems. It is worth notice that this type of simulations are collisionless, which means that the particles do not collide with each other. This characteristic does not have any impact since the DM halos and dynamics of high number of particles systems have a relaxation time much longer than the age of the universe and therefore can be considered collisionless systems (see J. Binney and S. Tremaine (2008)[15]) .

To integrate in time the equations of motion it is used the leapfrog scheme or Verlet method (Hockney & Eastwood, 1981, [2]). This method consist in updating the positions

and velocities at interleaved time points such that:

$$\begin{aligned} x^{(n+1)} &= x^{(n)} + v^{(n+\frac{1}{2})}\Delta t \\ v^{(n+\frac{1}{2})} &= v^{(n-\frac{1}{2})} + \frac{F(x^{(n)})}{m}\Delta t \end{aligned} \tag{2}$$

Where Δt is the time step and the n is the step number. Δt is adjusted to be small enough so the method is stable.

The simulations analyzed in this work have 3 types of particles :

- DM particles: These are the most massive particles in the simulations and represent the DM component which leads the formation of structures and rules over the barionic component.
- Gas particles: These are the particles that represent the barionic component of the Universe and are described with a set of properties such as temperature, chemical composition, density, degree of ionization i.e. These are affected by the hydrodynamic and radiative transfer methods and lead to the formation of the stellar component.
- Stellar particles: The stellar component in the simulation is formed when the gas component reach certain conditions of density and temperature that allow stellar formation to take place. Each stellar particle roughly represent a stellar population in a real galaxy since we do not have enough computing power to resolve individual stars, and they inherit the properties from the gas that comes from.

1.2 Gravity solver: Barnes-Hut algorithm

In the core of any N-Body simulation is the algorithm that computes the gravitational forces that each particle experiments. In this case, the code we use works with the Burns-Hut algorithm (J.Barnes & P.Hut [21]), which consists in creating an octree (as is shown in the figure 1 but in 3 dimensions), and in dividing the space in cells until we end up with a single particle in each cell. Then we just compute the individual forces for a particle with the closest neighbours and the rest of forces are treated as a multipole expansion or computed with the center of mass of the parent cell. In this way we reduce the computational complexity from $O(n^2)$ to just $O(nlog(n))$.

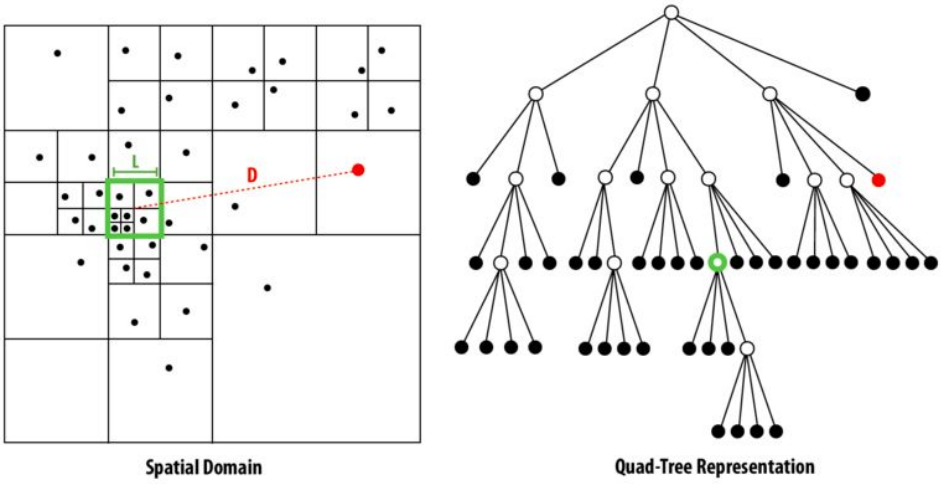

Figure 1: Illustration of a two dimensional oct-tree (quad-tree). The left panel shows the particles as dots and the spatial representation of the domains of each cell. The right panel shows the hierarchical structure that the tree follows. The orange line illustrates how the force between the orange particle and all the particles in the green cell is calculated without taking into account every individual particle. (credits to Parallel Computer Architecture and Programming)

1.3 Smooth particle hydrodynamics (SPH)

As we already know, the hydrodynamical interactions of the gas play a key role in the formation and evolution of galaxies. As N-Body simulations do not have a fixed domain divided in cells as classical hydrodynamical simulations do, Smooth Particle Hydrodynamics (SPH) is a way of approximating the continuum dynamics of fluids through the use of particles, which act as interpolation points. As we are working with moving particles, the Lagrangian formulation arises and SPH happens to be a formulation that conserves energy, momentum, mass and entropy simultaneously. In addition, since the particles follow the mass flow, we can adapt the resolution to capture the large density contrasts encountered in the Astrophysical simulations.

SPH formalism developed by Lucy (1977) and Gingold and Monaghan (1977) [3][4] is based on the discretization of physical quantities through what is called a kernel interpolant. It consists in computing the physical properties of the particle by summing the relevant properties of the neibourghs weighted by this kernel function. In this way for any quantity we can define a 'smoothed' one as:

$$F_s(r) = \int F(r)W(r-r',h)dr' \simeq \sum_j \frac{m_j}{\rho_j} F_j W(r-r_j,h) \tag{3}$$

Where W is the kernel function that has as inputs the smoothing length h (that varies to adapt the resolution) and the distance between the point and the particle $r - r_j$. For each point, we also have a mass m_i and density ρ_i , such $dr \sim m_i/\rho_i$ is their associated

finite volume element. From there, we can apply the Lagrangian formalism to a set of N particles and obtain the equations of motion as showed in Hopkins, 2013 [5] and that's are for the Euler equations:

$$\frac{dv}{dt} = -\frac{\nabla P}{\rho} - \nabla\Phi \quad \Rightarrow \quad \frac{dv_i}{dt} = -\sum_{j=1}^{N} m_j \left[f_i \frac{p_i}{\rho_i^2} \nabla_i W(r_{ij}, h_i) + f_j \frac{p_j}{\rho_j^2} \nabla_j W(r_{ij}, h_j) \right] \tag{4}$$

With f_i defined as $f_i = \left[1 + \frac{h_i}{3\rho_i} \frac{\partial \rho_i}{\partial h_i}\right]$. The density estimator automatically fulfills the continuity equation by construction:

$$\rho_i = \sum_{j=1}^{N} m_j W(r_{ij}, h_i) \quad \Rightarrow \quad P_i = (\gamma - 1)\rho_i u_i \tag{5}$$

It also automatically fulfils the energy equation for a reversible gas because the particle masses and their specific entropies (or thermal energy) remain constant for reversible gas dynamics. However, if we want to be able to form shocks we need to introduce artificial viscosity to the equation 4 and allow time integration to the entropies (or thermal energies) of the particles. We need then the equation of the thermal energy that reads as:

$$\frac{du}{dt} = -\frac{P}{\rho}\nabla v \quad \Rightarrow \quad \frac{du_i}{dt} = f_i \frac{P_i}{\rho} \sum_{j=1}^{N} m_j (v_i - v_j) \nabla W(r_{ij}, h_j) \tag{6}$$

With these equations we have the complete recipe to compute the hydrodynamics of our set of particles which, added to the gravity solver, the star formation and the radiative feedback, will give us the scheme of the simulation.

1.4 Star formation and chemical evolution

The last component to properly describe a galaxy is the stellar component, which provides the photons (along with gas) that allow us to actually see the structure and evolution. Many methods have been proposed to convert gas into stars in simulations (Yepes et al. 1997 [9]; Springel & Hernquist 2003 [11] i.e.), but the code we use follow Stinson et. al. 2018 [6] based on Katz 1992 [7]. This method selects the gas particles which fulfill a criteria. Then, among these particles, the actual star formation is set probabilistically in a way that on average we reproduce a star formation rate (SFR) close to a Schmidt law (Schmidt 1959[13]). The star particles inherit the velocity, position and metallicity of the parent gas particle, and have a predetermined mass that it is subtracted from the parent particle.

The criteria for being suitable to form stars are:

- The gas particle is denser than $n_{min} = 0.1\ cm^{-3}$
- The gas particle is in an overdense region $\rho/\bar{\rho} \geq 55$. Where $\bar{\rho}$ is the mean density.

- The gas particle must be part of a converging flow. Or in other words, the gas forming a star should be in a collapsing region.
- The gas particle must be Jeans unstable ($\frac{h_i}{c_i} > \frac{1}{\sqrt{4\pi G\rho_i}}$)

Since we do not reach the resolution to have individual star particles, each star particle represents (and therefore have the mass of) a stellar population with a fixed initial mass function (IMF). We used a Chabrier (2003) [24] initial mass function. The star particles then evolve giving feedback to the surrounding gas, injecting energy from stellar winds and supernova type II and type Ia. This feedback slows down (or stops) the star formation of the gas and enriches the medium with the processed material of the stars, providing the galaxies with the ability to evolve chemically depending on their SFR.

1.5 Stellar and black hole feedback

The stars not only give us most of the radiation that we observe in galaxies, but they also play a key role in galaxy and star formation. The feedback from stellar objects through supernova type II and Ia and the stellar winds from planetary nebulae allows the metals produced in our stars to be distributed and the energy of the feedback pushes and reheats the gas.

This allows the chemical evolution process to occur and self regulates the star formation since too much star formation leads to a strong feedback that pushes away the gas and heats it preventing it to continue forming stars. This process allows the star formation history of the resulting galaxy to have a more realistic structure.

The number of supernovae (SN), and therefore the amount of feedback that is produced by a stellar particle, depends on the IMF of the stellar population that the particle contains. As each particle contains a whole stellar population, a fixed IMF is used to compute approximately what number of stars will have each mass. Then their lifetime is computed depending on its metallicity and mass, following a previous parametrization. Once we know when the stars are going to explode we can compute the energy that they are going to introduce to the ISM by doing a integration to the IMF. Since the SNs usually occur where the gas has a high average density, the gas could radiate the energy introduced by the feedback in less than a timestep. To prevent that, and to proper mimic Blastwaves (since we can not resolve the multiphase of the ISM), we switch off the gas radiative cooling. Each gas particle surrounding the SN has its cooling disabled for a different period of time, depending on how much energy has received. These techniques also ensure the heating of the surrounding gas. The energy, mass and chemical elements released by the supernovae are smoothed out over the SPH kernel and the energy is introduced following a exponential rule.

Stars between 8 and 40 $M_\odot$ explode as SN-II, stars more massive than this are assumed to explode as type Ib SN. On the other hand, the SN-Ia are binary systems with a mass between 3 and 16 $M_\odot$ and make a 10-20% out of the total SN (see Greg Stinson et. al.

2018 [6] for more details about the feedback mechanism). For the stellar winds, a certain mass of the initial stellar mass is gradually returned to the ISM and smoothed over the SPH kernel with the same metallicity as the stellar particle but without the injection of energy. The total fraction of mass lost from a star particle over $> 10Gyr$ is 40% and of this $\sim$ 99% of the mass loss results from stellar winds (Greg Stinson et. al. 2018 [6]). This allows further star formation in galaxies without major gas inflows since the winds can stay within the virial radius of the galaxy.

Black holes (BH), or its seeds, are formed in a similar way as the star particles but with a more strict criteria.Specifically, BHs are formed when a gas particle meets the criteria to form stars and it also meets (see M. Tremmel et. al. 2017 [27] for more details):

- Low-mass fraction of metals ($Z < 3 \cdot 10^{-4} Z_{\odot}$).
- Density 15 times larger than the SF threshold.
- Temperature between 9500 and $10000K$.

This allows BH to form just if the gas is collapsing quickly enough and it is cooling relatively slowly. Once the BH are formed, they are allowed to accrete mass from the surrounding gas particles and imparting the energy from the accreted gas into the nearest gas particle isotropically via a smoothing kernel. The accretion algorithm takes into account the angular momentum of the gas at the resolved scales.

Black holes are also allowed to merge if they are sufficiently close (less than 2 smoothing lengths) and gravitationally bound (with low enough relative velocities). The dynamics between them and the other star particles are rather complex and take into account the dynamical friction that leads the BH to end up in the center of the galaxies.

Regarding the actual feedback model, to make sure the energy is dissipated realistically, the cooling of the surrounding gas particles is switch off for a time equal to the timestep of the BH (usually $10^3 - 10^4 yr$) like in Blastwave of the SNe but with different duration to account for the continuous accretion (see M. Tremmel et. al. 2017 [27] for an in depth explanation).

Considering the spatial resolution of our simulation, the kinetic energy that could be deposited by the feedback (both of the BH and stellar) will be dissipated into thermal energy within a smaller scale than our resolution limit. For that reason, all the feedback of the model is thermal and there is no explicit addition of kinetic energy in any of these simulations.

1.6 CHANGA Code

The code used for this work is ChaNGa (Thomas Quinn 2013 [18], P. Jetley et. al. 2008 [16], Harshitha Menon et. al. 2015 [17], M. Tremmel et. al. 2017 [27]), a parallel N-Body and SPH solver which is specifically designed for cosmological simulations of galaxy formation. It is capable of running a wide range of gravitational or hydrodynamical

problems. The key aspect of ChaNGa is that is based on the charm++ parallelization framework, which allows it to scale really efficiently up to $2 \cdot 10^9$ cores. The gravity and SPH algorithms used in the code are based on the previous code for cosmological simulations Gasoline (Wadsley, J. W. et. al. [12]).

The version of ChaNGa that we are going to use is the one implemented by M. Tremmel et. al in (Harshitha Menon et. al. 2018 [19]) which has the unique distinctive of having black hole physics (both interaction and feedback).

1.7 NIHAO and MAGICC simulations

As one of the goals of this work is to analyse previous simulations and to try to understand the differences in chemical evolution between galaxies, we will use the simulations from NIHAO and MAGICC projects. NIHAO (Numerical Investigation of a Hundred Astrophysical Objects, Liang Wang et.al. 2016 [14]) provides 100 cosmological zoom-in hydrodynamical simulations performed with the parent code of ChaNGa, Gasoline. MaGICC (Making Galaxies in a Cosmological Context, G. S. Stinson 2013 [28]) is very close in terms of parameters, code and cosmology to the NIHAO but has a different sample of galaxies and a different purpose.

The NIHAO project's aim is to create a large sample of galaxies with very high resolution over a wide range of halo masses with an unbiased sampling of the mass accretion histories (Liang Wang et. al. 2016 [14]). It covers a wide range of masses (from $M_{200} \sim 5 \cdot 10^9 M_\odot$ to $M_{200} \sim 2 \cdot 10^{12} M_\odot$) and with different star formation histories (SFH), star formation efficiency (SFE, defined as the SFR divided by the total mass of gas at that time) and merger histories, which allow us to study how these factors affect the final chemical abundances.

The MaGiCC simulation had the objective of introduce a model of early stellar feedback combined with SN feedback to match the stellar mass vs. halo mass relationship. One of the keys of the MaGICC project is to introduce a novel source of feedback that is often ignored in cosmological simulations, that is the UV radiation from massive stars before they explode as SN. It is also particularly interesting since it is designed to mimic the characteristics of the Milky Way (MW) and therefore we can compare them and extract relevant results as shown by Chris B. Brook et.al. 2020 [26] and 2013 [30]. The simulation has a mass of $7 \times 10^{11} M_\odot$ also formed an exponential disk with a classical bulge with a central surface brightness of $\mu_i = 14$, a total face-on magnitude of $M_r = -21.7$ and $g - r$ colour of 0.62 (G.S.Stinson et. al. 2013 [28]).

These projects are done with the same ΛCDM cosmology and the same parameters (described in 3.3), but different initial conditions. Both projects have been shown to reproduce a wide range of observed properties and scaling relations as for example stellar-halo mass relation, size and rotation velocity (Buck et.al. [25], Stinson et.al. [28]).

2 Objectives

The main objectives of this work are:

2.1 Run novel BH feedback simulations

1. Deep comprehension of N-Body simulations theory and what makes it a powerful tool to study galaxy formation and evolution.

2. Set up in the La Palma supercomputer the environment to run a simulation with a preexisting code that has not been tested yet. We need to develop the software infrastructure needed in the computer, install the proper libraries and check for compatibility between different software.

3. Run a simulation to test that everything is functioning correctly and prepare the set up for a full local group simulation.

2.2 Analyze chemical content of existing NIHAO/MAGICC simulations

1. Analyze previous N-Body simulations of the NIHAO project (Liang Wang et. al. 2016 [14]) in order to find relevant trends in the chemical abundance of the alpha elements (O, Ne, Mg, Si, S, Ca) and metals that relate the star formation history (SFH) with the chemical abundances.

2. Search in NIHAO simulations clues that help to understand the different chemical abundances and physical properties the galaxies have. In particular, how the chemical abundances are related between dwarf galaxies or regular galaxies, and their interactions, like mergers or tidal stripping.

3 BH feedback simulations: Methodology and Results

In this section we are going to discuss the main procedures and techniques used in the implementation of the new simulations, the programs used (3.2, 3.5), the computing facilities (3.1), as well as the preliminary results obtained (3.6).

3.1 Hardware used: La Palma supercomputer

As running and processing a simulation requires a lot of computing, power we were given access to the La Palma supercomputer, one of the IAC's computing facilities integrated in the Spanish supercomputing network (RES: *red española de supercomputación*). The machine has 252 nodes with 2 processors of 8 cores each, with a total of 4032 cores, 4TB of RAM and 346 TB of storage memory. Each node has 32 Gb of RAM giving 2 GB of RAM per process. We were given 3 million CPU hours by the IAC in order to run and process the simulation.

Of this computer we have used a maximum of 1024 cores simultaneously with execution times varying from 30 minutes to 72 hours, depending on the stage of the simulation we were at (i.e. debugging, testing, executing...).

La Palma supercomputer was also used (as well as another supercomputer in Abudhabi managed by the New York University) to access the data of previous simulation as well as to perform the analysis.

3.2 Installation and debug of ChaNGa

In order to run the simulation we need to first develop the software infrastructure needed for the program to run properly. With that purpose, several libraries and dependencies have been installed in La Palma with the help of the suport team, some of them are: Charm++ library, Pynbody python package, AHF, Grackle cooling library and the main code ChaNGa.

The compilation of that modules has been done with special care to perform optimally in a supercomputer with the specific characteristics of the LaPalma.

Once everything was installed, the first tests were deployed and a process of executions and revisions started. Everything took place with the help of the developers of ChaNGa (mainly Tom Quin and Michel Tremel) to make ChaNGa run properly in our machine.

The first problem we faced was a incompatibility between the cooling module and the main version of the code. We solved it by changing the cooling module from grackle to one integrated in ChaNGa. Then, a machine specific compilation problem made us run out of memory when we tried to load the initial conditions. This was also solved by changing the parameters of the compilation for the MPI module responsible of the paralelization. After that, we had a problem with the initial parameters which caused that the simulation failed in forming BH properly. Furthermore, the saving system also failed at the saving of each snapshot what make us being constantly restarting the simulation manually. The

parameters problem was solved but the saving problem (that was actually a file system management issue) was a bit more challenging and it is still pending of a proper solution.

3.3 Initial conditions and parameters

For the initial conditions, the main goal was to use the initial conditions of CLUES (Constrained Local UniversE Simulations, G. Yepes et. al. 2009 [31]) initial conditions for the local group of galaxies but, since they are too big to test with, we started with a dwarf galaxy taking the IC of one of the NIHAO's dwarfs (`g1.08e11`)(Liang Wang et. al. 2016 [14]).

Some of the properties of the initial conditions are:

- Number of particles: $N_{DM} \sim 3.33 \cdot 10^6$, $N_{gas} \sim 1.8 \cdot 10^6$.
- Box size: $8.24 \cdot 10^2 Kpc$
- Initial time: $1.76 \cdot 10^{-2} Gyr$
- Mass of the resulting galaxy: $M_{gas} = 4 \cdot 10^9 M_\odot$, $M_* = 5.8 \cdot 10^8 M_\odot$, and total mass of $M = 8 \cdot 10^{10} M_\odot$

The process of making a initial conditions for a zoom-in cosmological simulation is as follows.

Firstly, we need to have a cosmological model. In this case a ΛCDM model is used with the parameters of the plank collaboration (Plank collaboration et. al. 2019 [1]): Hubble parameter $H_0 = 67.1\ km\ s^{-1}\ Mpc^{-1}$, matter density $\Omega_m = 0.3175$, dark energy density $\Omega_\lambda = 1 - \Omega_m - \Omega_r = 0.6824$, radiation density $\Omega_r = 0.00008$, baryon density $\Omega_b = 0.0490$, power spectrum normalization $\sigma_8 = 0.8344$, power spectrum slope $n = 0.9624$.

Then, a cosmological simulation is performed and from there an unbiased sample of galaxies are selected with the condition of having isolated halos (i.e. no other halo with mass grater that 1/5 of the virial mass of the within 3 virial radii, described in Liang Wang et. al. 2016 [14]). Once we have the selection, we trace back the particles of our selected halo and resimulate them with the desired resolution and the techniques mentioned above.

3.4 Executions

For running ChaNGa, different execution models were created in order to test their performance as well as to test the difference between the models with and without BH. It is worth mentioning that the IC of all the runs and the cosmological parameters are the same so the spatial resolution is preserved betweeen runs and we can isolate the effect of the thing to study (i.e. BH feedbacks effects or currently time integration differences and structure formation hierarchy).

The first model that was executed was one with time resolution of $\Delta t \approx 0.02\ Gyr$. It needed a few restarts from several checkpoints (since we have technical issues mentioned

in the section 3.2). Alternatively, we ran another model with the same parameters but with much less time resolution ($\Delta t \approx 0.2Gyr$), which allowed us to have bigger steps in the time integration, to advance faster and to consume less computing resources. The previous model was compared with the high resolution one to see that the time integration and results were consistent between the different step sizes. They are not identical since this simulations have a stochastical component due to their chaotical nature (Keller, B. W. et. al. 2019 [10]). Furthermore, a model with BH and limited time resolution was executed to compare the results with the other two.

Due to time and technical reasons, all simulations are currently at $T \approx 2Gyr$ or $z \approx 3$ and have not reached $z = 0$, we discuss the results in the section 3.6

3.5 Halo finder

Once the simulation is completed, we end up with a picture of where each particle is located and its properties. Now to identify where the galaxies are, we apply to the snapshots a halo finder. In this case, we use Amiga's Halo Finder (Steffen R. Knollmann & Alexander Knebe 2009 [23]). What AHF does is identifying the structure of halos and subhalos looking for overdense regions. Then it computes which particles belong to the halo discarding the particles that are not gravitationally bound to it. Finally, it computes the virial radius and the other halo properties and makes a tree with the hierarchy of the halos. This allows us to easily analyse the galaxies within the simulation knowing where they are located (since we know the barionic structures are located inside the DM halos) and the gas, DM and stars that each one contains.

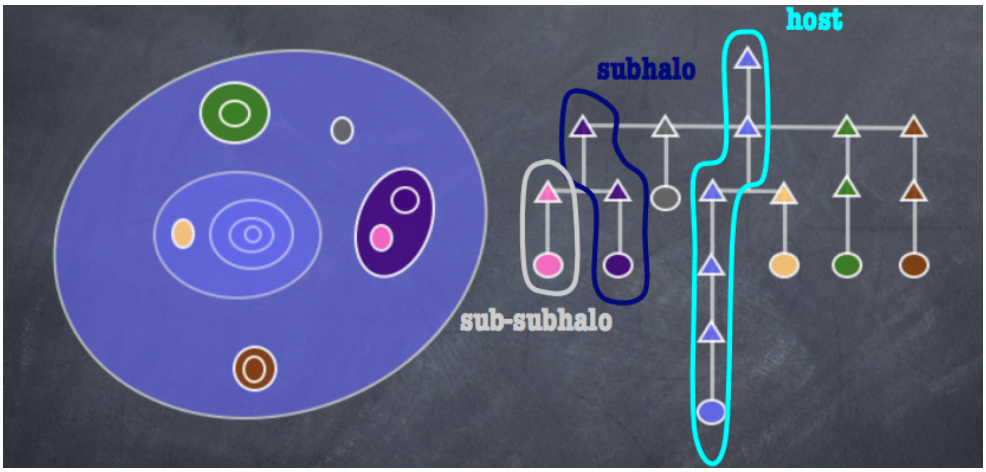

Figure 2: Structure of halos and subshalos formed by AHF software. The left side represents the isodensity curves that represent the mass gradients of a halo. The right side represents how the densities of the halo are translated to a hierarchical structure (Credits to AHF documentation).

3.6 Output of the simulations

Here we show some aspects of the different runs of the simulation. First of all, we performed a visual inspection over the different snapshots rendering the same image to compare them and to ensure that they are consistent (with the different integration steps). In figure 3 we can see that the different integration steps do not affect significantly the final output. Being the stellar mass of the different runs: High resolution $M_* = 1.70 \cdot 10^9$, low resolution $M_* = 2.22 \cdot 10^9$ at $z \sim 3$. That is because the code ensures that each step is subdivided in a way that the information is preserved through the integration.

We also made a movie showing the time evolution of the simulation with higher time resolution to see how the structures were formed and evolved (view it in this link: https://www.youtube.com/watch?v=_RdHdFuvLdc). As we are using a ΛCDM cosmology, we can see that the structures are formed in a bottom up hierarchy. The figure 4 shows different times to illustrate this.

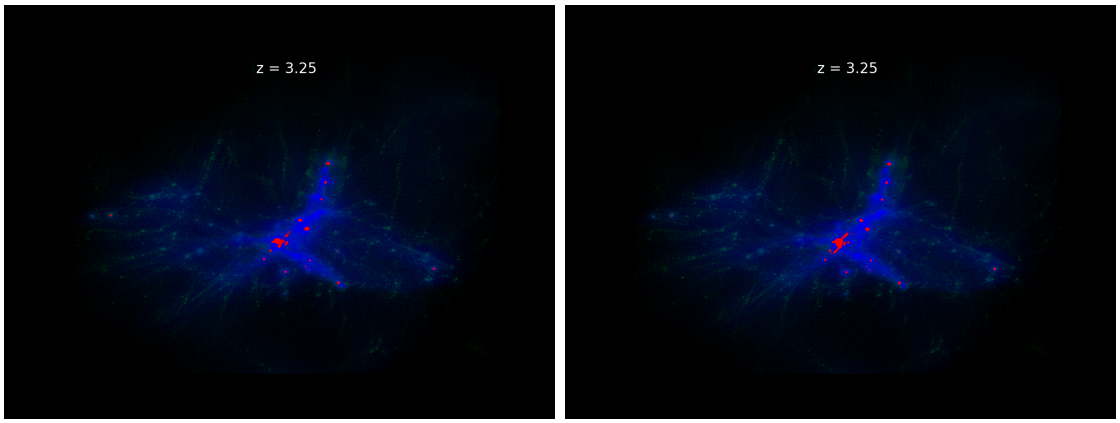

Figure 3: Comparison between the simulation with low time resolution (left) and high resolution (right). The blue dots are gas particles, the red dots are star particles. We can see that they are almost identical aside from a few difference due to numeric error (stellar masses of: High resolution $M_* = 1.70 \cdot 10^9$, low resolution $M_* = 2.22 \cdot 10^9$ at $z \sim 3$).

Therefore, we conclude that the implemented code is working properly and that is providing meaningful results. We are confident that in the near future we will be able to use it to perform large scale Local Group simulations.

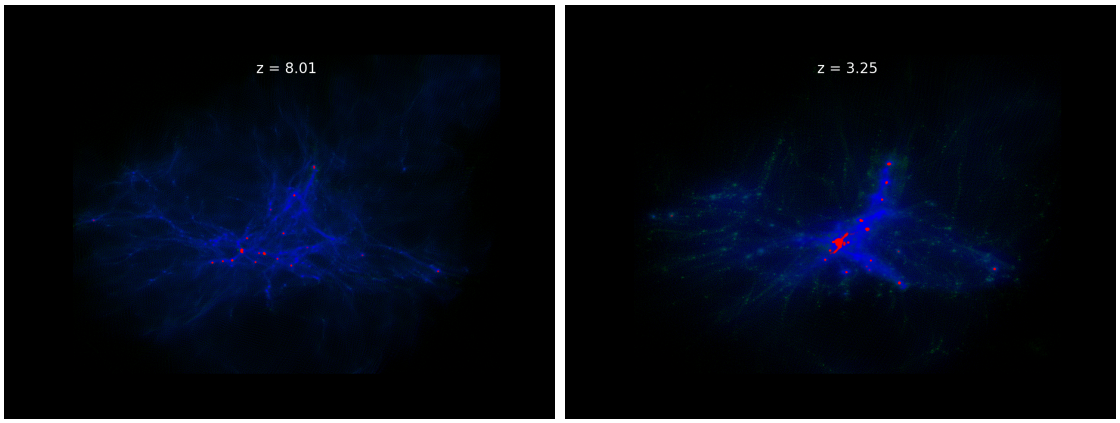

Figure 4: Different times of the simulation with high time resolution to see how different structures are formed.

4 Chemical content and SFH of NIHAO/MAGICC simulations: Methodology and Results

Now we present the second part of this work that consist in analysing previous simulations (NIHAO and MAGICC) and searching for links between SFH and chemical content, as well as showing how assembling history events relate with these features. We describe how the sample selection was made (4.1), the method used to analyse the data (4.2) and the main results (4.3, 4.4).

4.1 Sample selection

We chose the sample in different ranges of masses to do the analysis. We then had 3 subsamples: 2 Milky way like (MW,$M_{halo} \sim 10^{12} M_{\odot}$: `g1.92e12` and `g15684`), 2 small galaxies ($M_{halo} \sim 10^{11} M_{\odot}$: `g3.55e11` and `g2.39e11`) and 2 dwarfs (DW, $M_{halo} \sim 10^{10} M_{\odot}$: `g1.09e10` and `g2.09e10`).

We selected it in a way that the less massive galaxies have enough star particles to have a reasonable statistics and in the MW like we chose the ones that more resemble the actual MW.

In particular, the MAGICC simulation, with almost identical parameters as described in the NIHAO sample (it is also a zoom-in hydrodinamical simulation with the same code and the same cosmologies, SF parameters... etc), resembles the MW in merger history and other parameters (Brook et. al. 2020 [26]). The selected galaxies are:

- NIHAO sample: `g1.92e12`, `g1.77e12`, `g8.26e11`, `g3.55e11`, `g2.39e11`, `g2.41e11`, `g2.09e10`, `g1.09e10`. With a resolution (at $z = 0$) of: $N_{DM} \sim 3 - 5 \cdot 10^6$, $N_{gas} \sim 1 - 3 \cdot 10^6$, $N_{stars} \sim 1 - 10 \cdot 10^4$. With mean masses of particles: $M_{DM} \sim 2 - 85 \cdot 10^8 M_{\odot}$, $M_{gas} \sim 3 - 40 \cdot 10^3 M_{\odot}$, $M_{stars} \sim 7 - 648 \cdot 10^2 M_{\odot}$. From which `g2.39e11`, `g8.26e11`

and `g1.92e12` are shown in the appendix, since they are either similar to the ones already presented or have incomplete data.

- MAGICC sample: `g15684`. Some of the data about the resolution of this sample (at $z = 0$) is: Number of particles: $N_{DM} \sim 5.25 \cdot 10^6$, $N_{gas} \sim 1.28 \cdot 10^6$, $N_{stars} \sim 2.15 \cdot 10^6$ with mean masses of particles: $M_{DM} \sim 2.15 \cdot 10^9 M_\odot$, $M_{gas} \sim 2.08 \cdot 10^5 M_\odot$, $M_{stars} \sim 3.8 \cdot 10^4 M_\odot$.

As we are dealing with simulated galaxies, we have a snapshot of the simulations at different times. In the case of our simulations, the time resolution of the snapshots is every $\Delta t = 0.2\ Gyr$.

4.2 Analysis

For the analysis we have used the pynbody python package (Pontzen A. et. al 2013 [20]), which loads the snapshot of the simulation as well as the identifications of the halos done by the AHF and allows a easy manipulation of the simulation. The main steps of the analysis are:

- Loading the snapshot of the desired galaxy in the desired timestep corresponding to a particular time in the simulation.
- Identifying the main halo corresponding to the studied galaxy.
- Selecting the particles that are inside the virial radius of the galaxy and/or do a particular selection of particles (like the ones belonging to the disk of the galaxy or a particular anulus to resemble the solar neighborhood)
- Accessing the particles and extract the SFE, SFR, histograms of the $[O/Fe]-[Fe/H]$ plane, the mean chemical content and store it.
- Closing the snapshot and repeat with the other time steps of the same galaxy to have a full history of the chemical evolution of the galaxy.
- Representing the SFH and SFE of the galaxy at each timestep together.
- Repeating with the other galaxies in the sample

Several Python routines were written to perform this analysis and where executed in La Palma supercomputer as well as in other supercomputing facilities in Abudhabi. One for the Sample selection, computing the total mass, stellar mass, and the 2 dimension histogram in the $[O/Fe] - [Fe/H]$ plane to select the interesting galaxies that have the desired characteristics. The 2d histograms at $z = 0$ is what we could be able to observe (with different resolution and some constrains) and what is trying to be linked with the SFH and the merger history of the analysed galaxies. Another routine in python has been developed to compute the SFRs, SFE, alpha and metal content, total stellar mass,

gas mass and HI mass of each timestep in every analysed galaxy (from the ones selected earlier). The last routine is for representing the results of the previous analysis and to compare them, resulting in the figures 8 and 9.

The main computing load of the analysis is centred in the selection and manipulation of the right particles at the calculus of the SFR and other properties of the snapshots. Since the simulation has around $\sim 9 \cdot 10^6$ particles and the main halos studied around $\sim 1-4 \cdot 10^6$ particles (each particle with its own properties), it ends up in a big memory consumption. This present a challenge and has conditioned the way the routines are written and executed in order to optimise the resources available for the analysis.

4.3 Metals and alpha content

The relevant feature at which we are going to be looking at in our analysis is the distribution of the chemical content of the stars at $z = 0$. If the age of the stars is also taken into account, these properties reveal the chemical enrichment history of the galaxy, and how its metallicity and alpha content has evolved. The goal is to see how such properties depend on mass, and whether they reflect the formation history of the galaxies, including their merger histories, baryon cycle and star formation histories.

In figure 5 we plot the metallicity, specifically [Fe/H], as a function of age. We can see that the general trend is to increase the amount of metals with time, from left to right in the plots, (being the Fe the proxy) in all the galaxies of the sample, as it can be expected. This representation also allows us to see the merger history of the galaxies. When a merger occurs, the accreted stars generally have lower metallicity than stars in the main progenitor, because of the difference in masses between them. That leads to a different SFE as we will see.
This can be seen in the figure 5 top left panel in the `g15784` at 11 Gyr, where we can clearly see a merger where a lower metallicity line appears, and also in the top right panel where multiple different accretion events take place. Given the many more accretion events that have taken place at the second MW like galaxy `g1.92e12`, also at later time, it is not surprising that this galaxy ends up having a much larger spherical component than the first galaxy. In general, a more active merger history leads to earlier morphological types at a given mass. (Toomre, A. 1977 [8]).

Trends in the Fe-age plane can indeed give us a hint about what kind of evolution a galaxy has faced and what type of galaxy it is. For example, the MW like galaxies (spirals) have a large metal enrichment rate in the $13 - 10$ Gyr corresponding to a rapid increase in the SFR (see fig. 5 and 8 top left panel and galaxies 1-2 of the appendix) and then a flat profile which corresponds to the epoch of thin disc formation and evolution. In contrast, the other MW does not have the later flat profile and it is continuously increasing metallicity. That can be the result of the perturbation of the disc (due to the mergers) that may lead to temporary suppression of the star formation that ends up happening later in

the life of the galaxy as we can see by the concentration of stars between 5 and 2.5 Gyr. Notice that, despite the different merger histories, the galaxies in the same range of masses ends up with a really similar metallicity at $T = 0\ Gyr$, telling us that the mass in one of the main driving factors of metal gas enrichment, that leads to different stars enrichment.

Less massive galaxies have almost a constant increase in the Fe-age corresponding to flatter SFE-SFR profile. That seems to be the representative behaviour of the simulation that we are analysing for this range of masses. Regarding the dwarfs, the bursts in SF make the Fe-age diagram discontinuous and the plateau in the $[Fe/H]$-age (as the gas enrichment is compensated by gas accretion) is caused by the general (descending) envelope in the SFE-SFR.

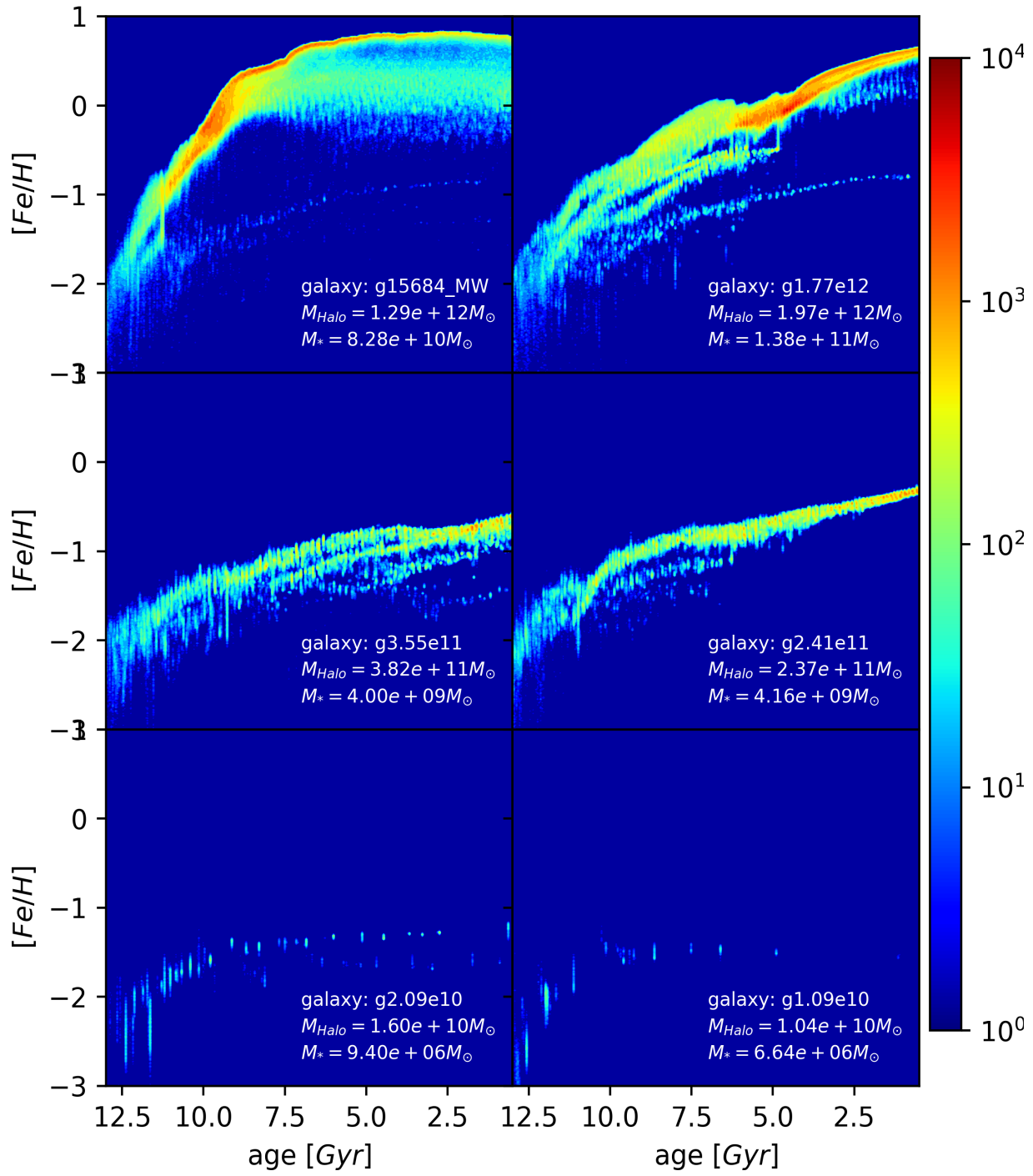

Figure 5: 2D histograms of the $[Fe/H]$-age relation of the stars at z=0. The sample is sorted by mass from left to right and from top to bottom: `g15684`, `g1.77e12`, `g3.55e11`, `g2.41e11`, `g2.09e10`, `g1.09e10`. Each row represents a subsample (MW,middle size and dwarf galaxies). The horizontal axis represents the age, being the right side z=0 and the left side the time 0 of the simulation, and the color represents the number of star particles in each bin of the $300x300$ grid in the parameter space.

Another relevant characteristic to look at is the alpha elements relative to the metal content of the stars (taking $[O/Fe]$ as a proxy) over time. In the Figure 6 we do a histogram of relative alpha content of stars, in particular $[O/Fe]$, with the age of those stars. The aim of this marker is to show the relation between SN type II and Ia. The SN II (or core collapse) are produced by the explosions of stars more massive than $10M_{\odot}$ and produce mainly alpha elements (and some Fe). On the other hand, the SN Ia are produced via deflagration of a white dwarf (WD) reaching the Chandrasekhar limit, destroying the whole star and producing a large amount of Fe ($\sim 0.5 - 0.7M_{\odot}$) (Cosmochemistry pg 223 [22]). The SN II occurs right after the SF happens (and therefore enrich the medium with alpha elements) because of the short life of the high mass stars, while the SN Ia appears "delayed" with respect to the formation of the star due to a much larger life of the smaller stars and the formation of binary systems.

Due to the different origin of the elements mentioned, we have that while the SFR decreases the $[O/Fe]$ content also decreases as the O formed depends on the current SF and the Fe depends on the SF occurred in a previous time (and vice versa when the SFR increases). It is also worth mentioning that, for the same reason, the $[O/Fe]$ will start high since the alpha elements are the first in being released after the first stars are formed. That situation happens in the most massive galaxies as we can see in the fig. 6 and the corresponding SFH supporting that claim will be discussed in the figure 8.

We can also see the same difference in the SF in the two MW mass galaxies as in the figure 5, where the bulk of SF in the first MW galaxy occurs in the $11 - 7.5\ Gyr$ and in the second one occurs in the $7 - 2.5\ Gyr$.

On the other hand, our subgroup of middle range masses (second row on that figure) has a flat $[O/Fe]$ evolution due to its relatively flat SFH leading to the creation of equal amounts of Fe and O. The bursts in SF of the DW with a decreasing trend in SF will lead to a decrease in $[O/Fe]$ during time. We can also notice that there are events that match both figures 5 and 6, for example important mergers or the start of the plateau in the first MW leave an imprint in the $[O/Fe]$ diagram at the same times as in the $[Fe/H]$.

If we combine the two chemical tracers that were selected, we end up with a sort of chemical phase space $[O/Fe] - [Fe/H]$. Which gives us information about how the SFH and merger history of the galaxy have been. This is particularly interesting since we can collect this data directly from observed galaxies (without any previous application of models), and infer therefore the possible SFH and merger history of that galaxy looking at this chemical plane. The figure 7 shows a 2D histogram of this parameter space formed by $[O/Fe]$ and $[Fe/H]$ of the stars at $z = 0$.

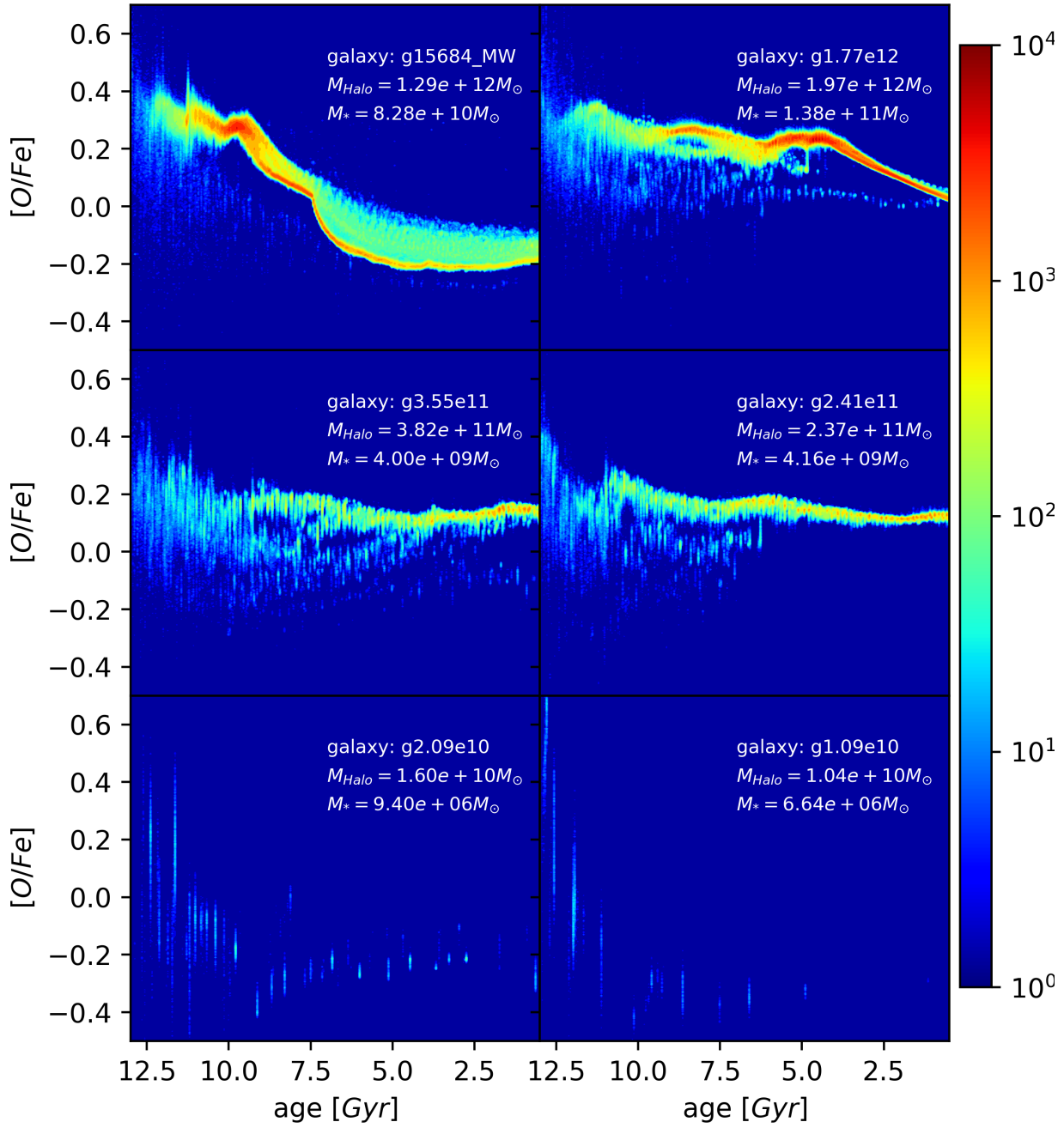

Figure 6: 2D histograms of the $[O/Fe]$ over age of the stars at z=0. The sample is sorted like in the figure 5.

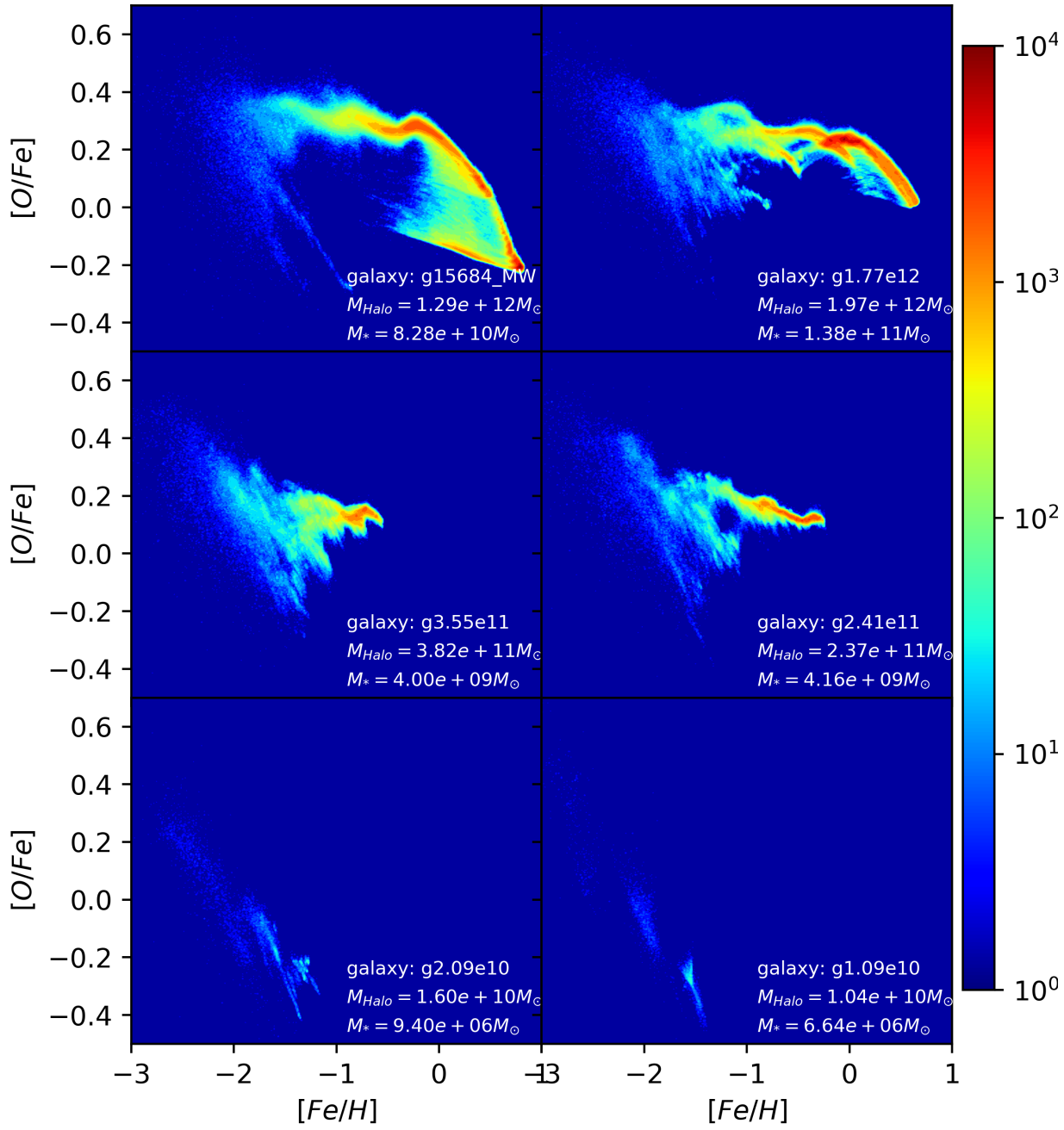

Figure 7: 2D histograms of the $[O/Fe]$ over $[Fe/H]$ of the stars at z=0. The sample is sorted like in the figure 5, and the age and color-bar are also equal to the figure 5 .

If we analyse the differences between the subgroups of the sample in the figure 7, we can see that there is a positive correlation between the mass and the relative content of metals $[Fe/H]$ and therefore the stars are shifted in the x axis. We can say therefore that, as we go higher in mass, the galaxies go further in the production of metals in the simulation.

Another way to look at the representation of the figure 7 is thinking in terms of gas pollution. So the x axis of the figure 7 ($[Fe/H]$) is a measure of how much the gas, which is predominantly made of hydrogen, is polluted. Therefore, galaxies with less stars relative to their gas content will become less polluted and the relation will be shifted to more negative values.

We have mentioned that more or less flat SFH relates to a flat $[O/Fe]$ profile for the middle mass group so we have that the enrichment have had to take place producing a more or less equal amount of O and Fe. That implies that the chemical plane of the galaxies in the middle range of masses in the figure (second row in figure 7) has to be populated from left to right (if the inflow of gas is sufficiently slow to not compensate the creation of metals). Regarding the dwarfs, we see the different SF bursts (explained in fig 8) tracing almost vertical lines with a low $[O/Fe]$ and also low metal content.

The time evolution and spatial change of this phase space has also been analysed in detail separately (videos here for the MAGICC galaxy: chemical evolution of the new born stars https://youtu.be/kG4xWRgCAo0 and radial change in the disc of the galaxy https://youtu.be/EuqMHFRMRLU). The relation between pollution timescales and star formation is related to the SFE. The SFE gives a sense of the timescale over which the gas will be consumed, assuming there is no fresh gas supply. Therefore, we therefore are motivated to explore the effects of star formation efficiency on the abundances of metals.

4.4 Star formation history and star formation efficiency

The star formation history of a galaxy gives us information about the age of the different stellar components present in a galaxy and how they have been created. If we compare the star formation efficiency (the amount of stars created divided by the available gas) with the SFR, we can see how the galaxy has incorporated the gas from the inflows. We can say that we can infer a sort of "accretion history" of gas combining the SFE and SFR.

Another key aspect of knowing the SFE of a galaxy is that this SFE over time give us information about how the previous SF regulates the current SF and how SF bursts affect the further creation of stars in our simulation and, in consequence (if the model is accurate), in the real universe.

As we mentioned earlier, the SFE is also related to the chemical abundances in the galaxy. Consequently, establishing relations between SFE and chemical abundances will be necessary if we want to infer the SFE of galaxies during their evolution with data from the chemical abundance plane.

The figure 8 shows the histogram of the different SFE (with all gas and with HI) and the corresponding line of the SFR over time, which constitutes the SFH of the galaxies.

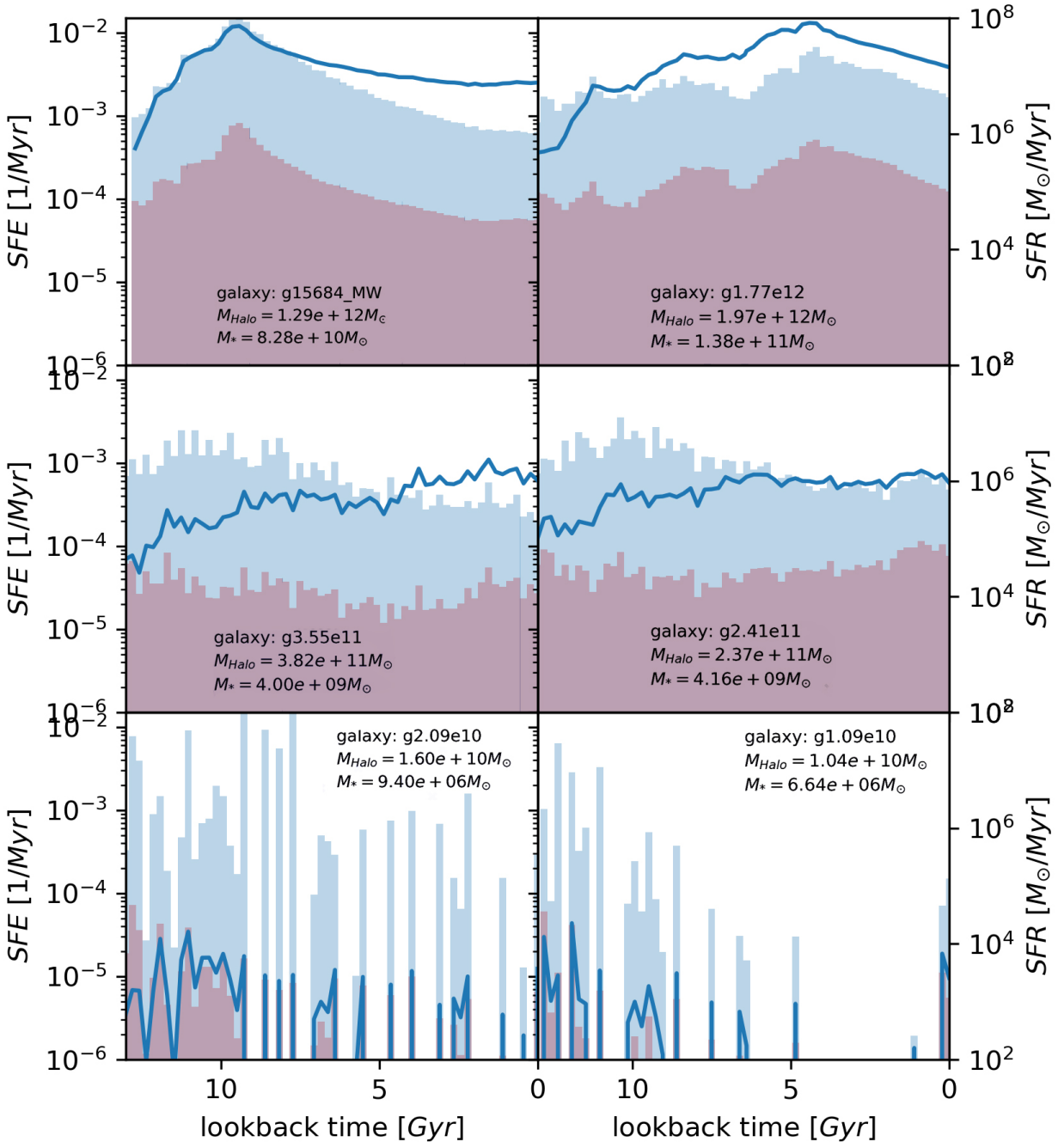

Figure 8: Histogram of the SFE (both "observationally" computed as $SFE = SFR/M_{HI}$ in blue and total as $SFE = SFR/M_{gas}$ in red) and SFR (blue line) of the sample of galaxies sorted like in the figure 5.

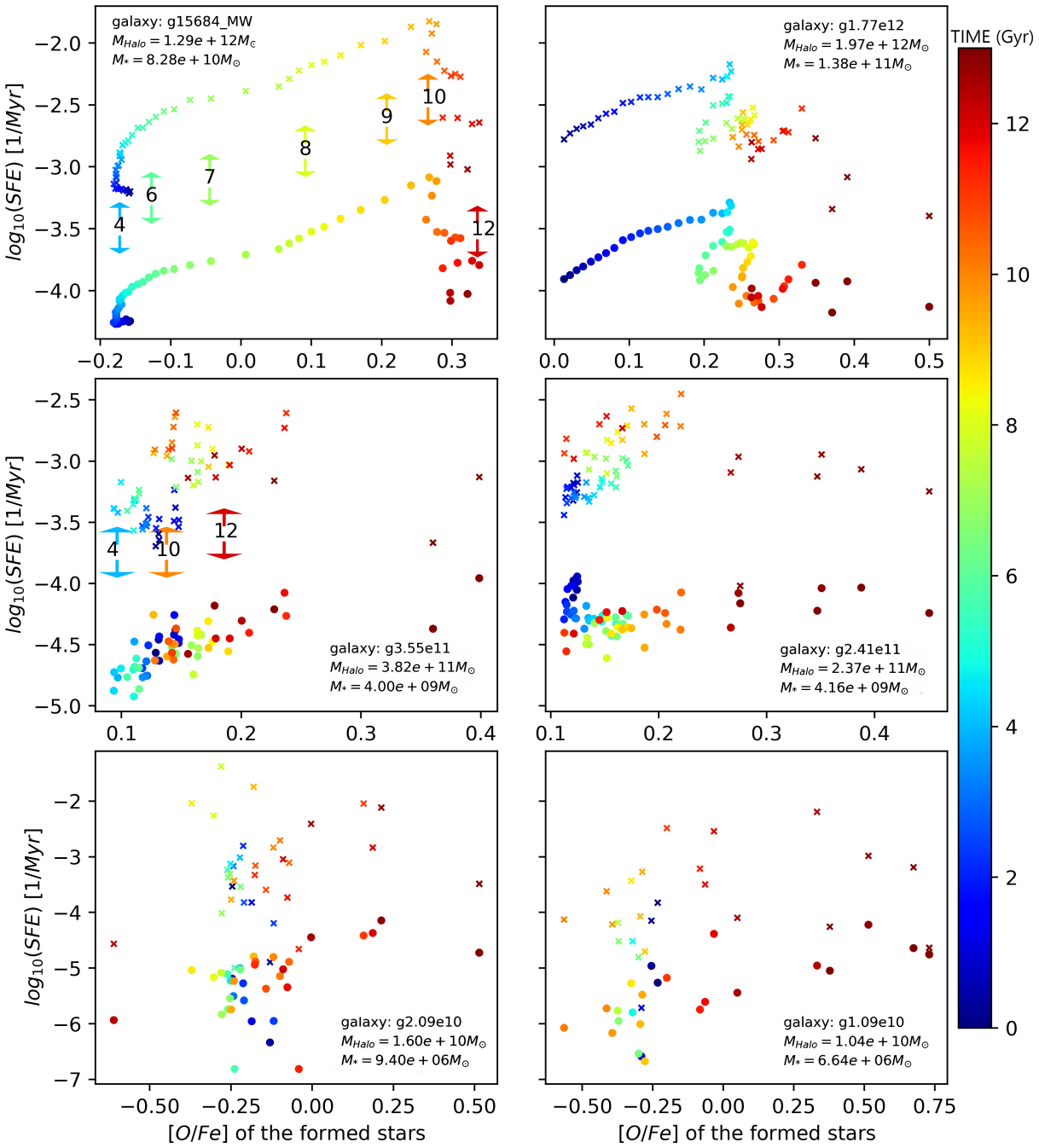

Figure 9: SFE ("observed" represented as crosses and total as dots) and $[O/Fe]$ relation color coded according to the time of the snapshot at which each points belongs to, where today is color blue, and the beginning of the simulation is color red (lookback time in Gyr). The arrows represent a interpolation of where a particular time is located in the $[O/Fe]$ axis to show how the $[O/Fe]$ is correlated with time depending of the mass of the galaxy. The galaxies are sorted like in the figure 5.

In the Figure 8 we can see that the mass is a critical aspect in defining the SFH of a galaxy. In addition, the second most important aspect is the merger history. In the top left we can see the typical MW galaxy (similar results have been found in the other MW like galaxies analysed in the appendix) with a peak in SF and then a slow decline in efficiency (but not in SFR) that indicates significant gas accretion. The other MW mass galaxy has more disturbance events (i.e mergers) that made the SFH less typical, but we can identify some of the events of mergers present in the figures 5 and 6 around 5 and 8 Gyr.

The middle range masses have more of a stable SFH that are almost flat, with a slow decline in the so called "observed" SFE (derived with the amount of HI gas instead of the total gas) and a slowly increasing SFR, which also indicates gas accretion.

The dwarfs have bursts of SF that lead to strong feedback (relative to their masses) and prevent further SF by heating the gas.

We can also compare the SFE with the $[O/Fe]$ content of the newly created stars ($age < 100\ Myr$). We show this in the figure 9, where the logarithm of the SFE is plotted versus the alpha content ($[O/Fe]$ as proxy) of the newly created stars. The colors show the time at which the point belongs to, so at each timestep we have a particular SFE with the alpha content of the created stars in that time, and repeating this for every snapshot in our simulations gives us the plots in the figure 9. The time coloring also illustrates the different relations of the $[O/Fe]$ content with time depending of the mass range of the galaxies that we are dealing with.

We can see how the SFE is positively correlated with the $[O/Fe]$, as already mentioned, because of the relation between different types of SN, clearly visible in the most massive galaxies. As we go down in masses, the relation between SFE and $[O/Fe]$ starts to vanish along with the relation between $[O/Fe]$ and time.

More massive galaxies will tend to have a decreasing $[O/Fe]$ with time, as seen in the figure 9, but when we go to lower masses this trend disappears. This is due to the particular relation between $[O/Fe]$ and time, since in earlier times more relative content of Oxygen is released but when the SN-Ia starts to dominate the release of Iron overtakes the Oxygen and starts to decrease the $[O/Fe]$. We can also relate that with the shape of the SFH, since the $[O/Fe]$ is correlated with time in the more massive galaxies, we can see how the top panels of the figure 9 resemble the SFH (inverted) of those galaxies. This relation appears from joining the figures 6 and 8.

5 Conclusion

The latest models of SN and BH feedback implemented in highly parallel codes (M. Tremmel et. al. 2017 [27], Thomas Quinn 2013 [18]) have made possible to simulate with unprecedented detail the formation and evolution of galaxies. This allows to propose a zoom-in cosmological simulation not only of isolated galaxies but also of an entire local group analog, in line with previous works like CLUES (N-Body simulation of a local group,G. Yepes et. al. 2009 [31]), in order to answer questions about the origin and evolution of the different components in the MW (as showed in Chris B. Brook et.al. 2020 [26]).

In the first part of this project, we successfully prepared the infrastructure in La Palma supercomputer to run the simulations in the following ways:

Installed pynbody python package, installed tipsy module, installed charm++ parallelization framework for C++ that uses MPI, compiled the ChaNGa code with the adequate parameters to run in our machine and installed Amiga Halo Finder.

We managed to get running to $z \sim 3$ the first tests of dwarf galaxies with the initial conditions of one of the NIHAO galaxies (`g1.08e11`, 1 of the 100 zoom-in cosmological simulations from MW to dwarfs, Liang Wang et. al. 2016 [14] with the characteristics described in 3.3). In these runs we got a good behaviour of structure formation independently of time resolution in the outputs (figures 3.6, 4 and Video) . These are the first steps to run a local group hydrodinamical simulation with all the physics mentioned in 1.3,1.5 and 1.4.

At the big scales, several models reproduce general galaxy properties such as stellar mass, luminosity function and morphology among others (Tobias Buck et. al. 2020 [25], Chris B. Brook et.al. 2020 [26]). But due to the impossibility of reaching such a high resolution to resolve individual stellar processes and the lack of comprehension of the first principles that drive this stellar processes (such as SF or feedback), there is a need of physical descriptions to implement sub-grid physics in the unresolved scales.

In order to analyse this sub-grid physic recipes, in the second part of the project we looked at the chemical abundances of simulated galaxies to provide constrains on the details of galaxy formation models. In particular, we looked at the previous simulations explained in the section 1.7 (MAGICC: G. S. Stinson et.al. 2013 [28], NIHAO: Liang Wang et. al. 2016 [14]). We selected a sample of 6 galaxies (5 NIHAO + 1 MAGICC) 2 Milky way like (MW,$M_{halo} \sim 10^{12} M_{\odot}$: `g1.92e12` and `g15684`), 2 small galaxies ($M_{halo} \sim 10^{11} M_{\odot}$: `g3.55e11` and `g2.39e11`) and 2 dwarfs (DW, $M_{halo} \sim 10^{11} M_{\odot}$: `g1.09e10` and `g2.09e10`). We chose this to have an unbiased sample in all the mass range and merger histories based on the enrichment history and the $[O/Fe]$-$[Fe/H]$ plane.

We analysed the results obtained by the previous models (MAGICC: G. S. Stinson

et.al. 2013 [28], NIHAO: Liang Wang et. al. 2016 [14]) with a particular sub-grid model, very close to what we implemented in the first part of the work. We found that SFH is related to the chemical enrichment history of the galaxy, more particularly, to the trend in the SFR, which determines the relative quantities of α elements and Fe due to the different proportions released by SN-Ia and SN-II. The mass of the galaxy also determines the SFH, making the MW like galaxies have a peak in the SFH that affects the way the $[O/Fe]$-age and $[Fe/H]$-age develops, while the smaller galaxies have a flatter SFH that ends up in a flatter $[O/Fe]$-age and $[Fe/H]$-age profiles (figures 6, 5 and 8). This gets reflected in the chemical plane of $[O/Fe]$-$[Fe/H]$, with the more massive galaxies developing further in the formation of metals and evolving to less relative content of α elements with respect to Fe than the low massive ones that have a flatter evolution in this chemical space (figure 7).

Another interesting finding is that the SFH, the mass and the assembling history of the galaxy are the main drivers of the chemical distribution in the stars at $z = 0$ in the simulations analysed. At the same time, mass and merger history are clearly related to the shape of the SFH, having each range of masses their particular characteristics:

- The MW like galaxies have (in general) a peak of SF around $10 - 12\ Gyr$ and then a slow decline. This is significantly affected by mergers that can delay this peak and affect the chemical evolution of the galaxy (as happens with `g1.92e12` visible in the top-right panel of the figures 8,6,5,9).
- Middle range mass galaxies have flat relations of $[O/Fe]$-age (figure 6),$[Fe/H]$-age (figure 5) and $[O/Fe]$-$[Fe/H]$ (figure 7), which indicates that they formed equal amounts of α elements and Fe. The SFE (figure 8) also indicates that these galaxies have an accretion rate (relative to their mass) of new gas closer to the MW galaxies than to the DW galaxies.
- Dwarfs have SF bursts that stop further SF and also have a general trend to decrease the SFH over time. Their $[O/Fe]$ content is monotonically decreasing, as a consequence of that decrease in SFR, although the SF burst make the general trend in the chemical plane discontinuous.

In addition, the dwarf galaxies seem to be much more influenced by feedback as the relative energy return is higher (since there is less material), and therefore, we can expect that SN feedback suppresses in a higher degree further SF. For this reason, it also ejects more gas out.

The results found in the galaxy `g15784` of the MAGICC sample during this work have led to conclude that the chemical trajectories can be related to the assembling history of the galaxy and can explain the origin of the different chemical abundances in the halo stars accreted and the ones born in situ in the MW (as we presented in Chris B. Brook et.al. 2020 [26]). This is due to the close match between this simulated galaxy and the actual history of the Milky Way.

6 Ongoing and future work

This work sets the basis to future simulations using the developed software infrastructure in the facilities mentioned in section 3.1. The project is currently active and now we are fine tuning the details to run a local group simulation with BH feedback with this implementation. Some technical problems need to be addressed first, but this work showed what need to be solved and bring us closer to the initial goal of running a proper zoom-in local group simulation with all the physics mentioned.

In the analysis section, we are now looking at the barion cycle and trying to see where the gas that formed the stars present at $z = 0$ has come from and how it has been enriched. Currently, we are developing a code that traces the gas particles (that has formed the current stars) back in the snapshots of the simulation to see the history of those particles. In the figure 10 we can see the velocity field of the gas particles in edge-on and face-on configurations, superposed to the line of sight density plot of those particles of one of the MAGICC galaxy. As we can see in the bottom left panel there is some of the particles that are ejected in what is called the *galactic fountain effect*. This consists in the recycling of blown-out gas that reenters the SF region later (see C.B. Brook et. al. 2014 [29]). Understanding how such galactic fountain acts in the formation of the galaxy is imperative, and it is the topic of our on-going work.

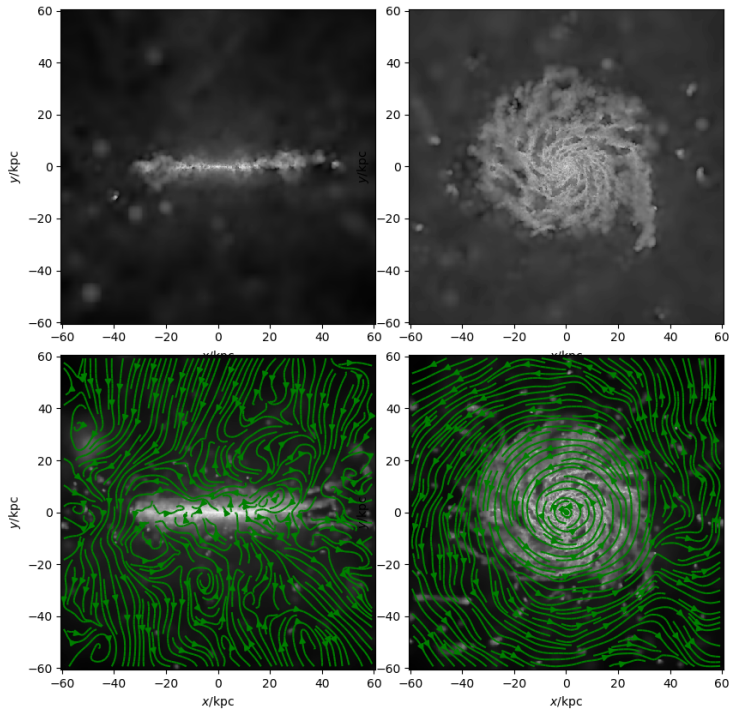

Figure 10: Galaxy `g15784` in the edge-on and face-on perspectives with a grey scale representing the gas density and superposed the velocity vector field of the gas particles.

References

[1] Plank collaboration et. al. 2019 "Planck 2018 results. VI. Cosmological parameters"
A&A September 24, 2019

[2] Hockney, R. W.; Eastwood, J. W. "Computer Simulation Using Particles"
New York: McGraw-Hill, 1981

[3] L. B. Lucy. "A numerical approach to the testing of the fission hypothesis."
The Astronomical Journal, december 1977.

[4] R. A. Gingold and J. J. Monaghan. "Smoothed particle hydrodynamics: theory and application to non-spherical stars."
Monthly Notices of the Royal Astronomical Society, december 1977

[5] Philip F. Hopkins "A General Class of Lagrangian Smoothed Particle Hydrodynamics. Methods and Implications for Fluid Mixing Problems"
Monthly Notices of the Royal Astronomical Society, June 2018

[6] Greg Stinson et.al. "Star Formation and Feedback in Smoothed Particle Hydrodynamic Simulations–I. Isolated Galaxies"
Monthly Notices of the Royal Astronomical Society, October 2018

[7] Neal Katz "Dissipational Galaxy formation. II. Efects of star formation"
The AstrophysicalJournal, 391:502-517,1992 June 1

[8] Toomre, A. "Theories of spiral structure.n"
The AstrophysicalJournal, 391:502-517,1992 June 1 Annual review of astronomy and astrophysics. Volume 15. (A78-16576 04-90) 1977

[9] G. Yepes et. al. "Hydrodynamical simulations of galaxy formation: effects of supernova feedback"
Monthly Notices of the Royal Astronomical Society, 1997

[10] Keller, B. W. et. al. "Chaos and variance in galaxy formation"
Monthly Notices of the Royal Astronomical Society, Volume 482, Issue 2, January 2019, Pages 2244–2261, https://doi.org/10.1093/mnras/sty2859

[11] Springel & Hernquist "An analytical model for the history of cosmic star formation"
Monthly Notices of the Royal Astronomical Society, 2003

[12] Wadsley J. W. et. al. "Gasoline: a flexible, parallel implementation of TreeSPH"
New Astronomy, Volume 9, Issue 2, p. 137-158

[13] Schmidt, Maarten "The Rate of Star Formation"
The Astrophysical Journal. 129: 243. Bibcode:1959ApJ...129..243S. doi:10.1086/146614.

[14] Liang Wang et. al. "NIHAO project I: Reproducing the inefficiency of galaxy formation across cosmic time with a large sample of cosmological hydrodynamical simulations."
Monthly Notices of the Royal Astronomical Society, November 2016

[15] James Binney and Scott Tremaine. "Galactic Dynamics"
Princeton University Press 1994

[16] P. Jetley, F. Gioachin, C. Mendes, L. V. Kale and T. Quinn. "Massively parallel cosmological simulations with ChaNGa,"
2008 IEEE International Symposium on Parallel and Distributed Processing, Miami, FL, 2008, pp. 1-12, doi: 10.1109/IPDPS.2008.4536319.

[17] Harshitha Menon et. al.. "Adaptive Techniques for Clustered N-Body Cosmological Simulations"
Computational Astrophysics and Cosmology, Volume 2, article id.1, 16 pp. March 2015

[18] Thomas Quinn. "The New Frontier of cosmological Simulations: Robust predictions of the galaxy population properties at z¿4"
HST Proposal ID 13264. Cycle 21

[19] Harshitha Menon et. al.. "Off the Beaten Path: A New Approach to Realistically Model The Orbital Decay of Supermassive Black Holes in Galaxy Formation Simulations"
Monthly Notices of the Royal Astronomical Society, 24 August 2018

[20] Pontzen A. et. al. "pynbody: Astrophysics Simulation Analysis for Python"
Astrophysics Source Code Library, 2013 ascl:1305.002

[21] J.Barnes & P.Hut. "A hierarchical O(N log N) force-calculation algorithm".
Nature. 324(4): 446–449. (December 1986)

[22] Cosmochemistry. "The melting pot of the elements".
Cambridge Contemporary Astrophysics.

[23] Steffen R. Knollmann & Alexander Knebe. "AHF: AMIGA'S HALO FINDER".
ApJS, 182, 608, 2009

[24] Gilles Chabrier. "GALACTIC STELLAR AND SUBSTELLAR INITIAL MASS FUNCTION "
Publications of the Astronomical Society of the Pacific, 115:763–795, 2003 July.

[25] Tobias Buck et. al.. "NIHAO-UHD: The properties of MW-like stellar disks in high resolution cosmological simulations"
MNRAS January 7, 2020.

[26] Chris B. Brook et.al. *Chris B. Brook et.al. 2020* "Explaining the chemical trajectories of accreted and in-situ halo stars of the Milky Way"
MNRAS April 2020.

[27] M. Tremmel et. al.. "The ROMULUS cosmological simulations: a physical approach to the formation, dynamics and accretion models of SMBHs"
MNRAS 470, 1121–1139 (2017)

[28] G. S. Stinson, C. Brook et. al.. "Making Galaxies in a Cosmological Context: The Need for Early Stellar Feedback"
MNRAS 428, 129–140 (2013)

[29] C. B. Brook et. al.. "MaGICC baryon cycle: the enrichment history of simulated disc galaxies"
MNRAS 443, 3809–3818 (2014)

[30] C. Brook et. al.. "The Lowest Metallicity Stars in the LMC: Clues from MaGICC Simulations"
PASA, Vol. 30

[31] G. Yepes et. al.. "The CLUES project: Constrained Local UniversE Simulations"
Conference Proceedings, Volume 1178, pp. 64-75 (2009).

A APPENDIX: Glossary of terms

We now expose the specific terms used during the work and their meaning:

AHF: Amiga Halo Finder.
DW: Dwarf galaxy.
DM: Dark matter.
IMF: Initial mass function.
ISM: Inter stellar medium.
$\mathbf{R_{500,200...}}$: Radii at which the density is 500 or 200 times the mean background density $\rho/\bar{\rho} = 500, 200$.
$\mathbf{M_{500,200...}}$: Mass within $R_{500,200...}$.
$\mathbf{M_{gas}}$: total amount of gas.
$\mathbf{M_{HI}}$: Mass of neutral atomic hydrogen .
MW: Milky way .
SFE: Efficiency in which the galaxy is forming stars, computed as the SFR divided by the amount of gas (total gas or HI gas).
SFH: Different rates at which new stars were formed (expressed in mass/time) at the different times.
SFR: Rate at which new stars are being formed (expressed in mass/time).
SN: Supernovae.
SPH: Smoothed Particle Hydrodynamics.

B APPENDIX: Other Analyzed Galaxies

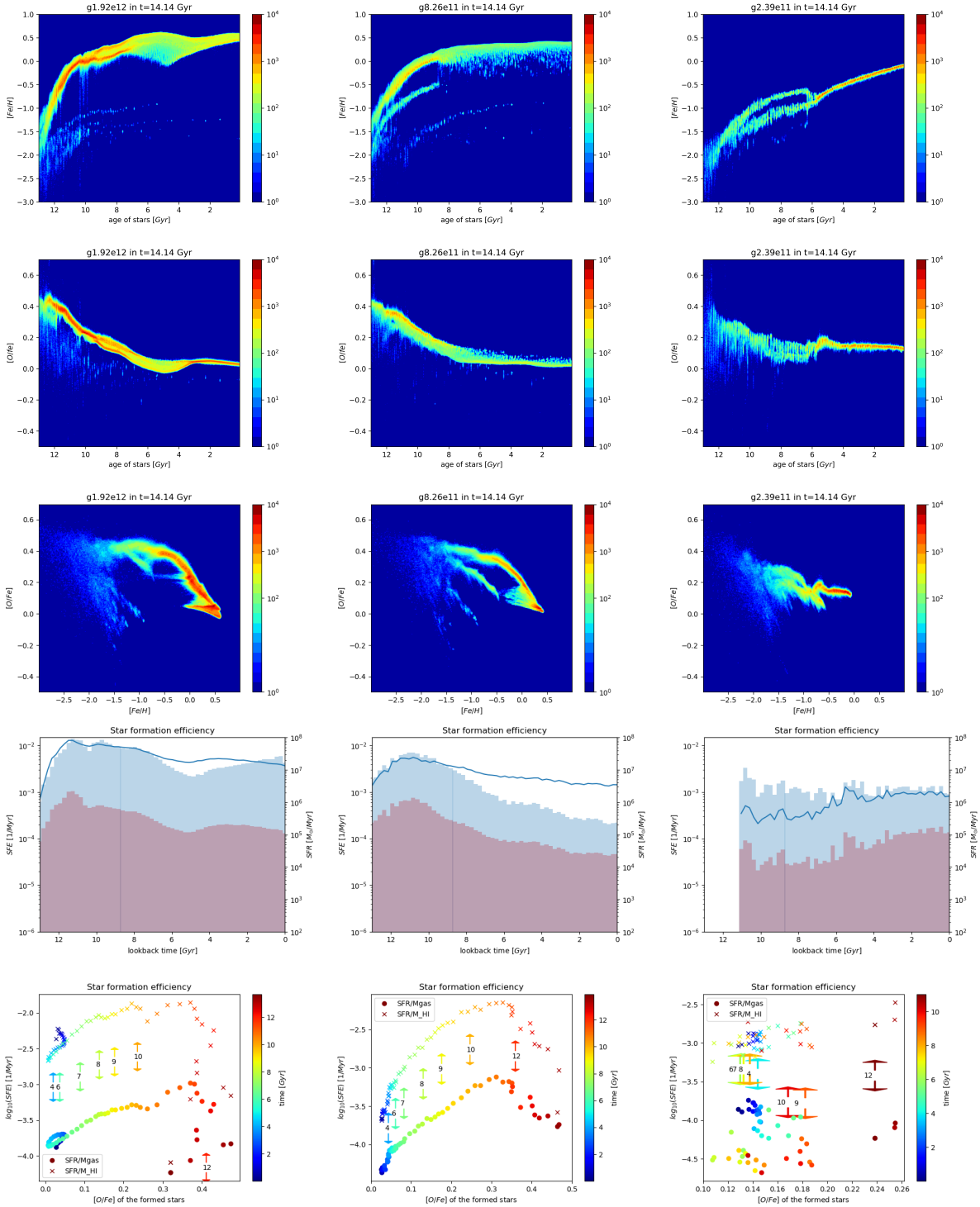

Figure 11: Caption